Time-Domain Precoding for LTE-over-Copper Systems

Yezi Huang*, Eduardo Medeiros*, Thomas Magesacher*, Stefan Höst*,
Chenguang Lu†, Per-Erik Eriksson†, Per Ödling* and Per Ola Börjesson*
*Department of Electrical and Information Technology, Lund University, Sweden
{firstname.surname}@eit.lth.se
†Ericsson Research, Kista, Sweden
{chenguang.lu, per-erik.s.eriksson}@ericsson.com

***Abstract*—Crosstalk cancellation is a crucial issue for traditional digital subscriber line systems. For LTE-over-copper systems, however, the need for crosstalk cancellation varies depending on the analog fronthauling architecture and its parameters. A crosstalk handler that is decoupled as much as possible from the rest of the system architecture is thus preferred. Therefore, we propose a time-domain precoding scheme specifically in downstream direction to separate the precoding unit from the LTE signal flow, and perform crosstalk cancellation in an on-demand manner. Estimation of all direct and crosstalk paths is assisted by LTE cell-specific reference signals. The time-domain precoder transforms the interference channel into a crosstalk-free channel with identical direct paths, which allows for low-complexity inter-symbol interference mitigation. We evaluate the concept in terms of signal-to-noise ratio provided for LTE signals using measured wireline channel data.**

I. Introduction

Small cells are promoted as an important enabler for high capacity indoor radio. However, fronthauling and backhauling that connect small cells to the core network turn out to be challenging due to the deploying locations and set-up cost per user. Reusing fixed broadband networks in this regard can be an economic solution to achieve the small cell densification.

In [1], a femto-wireless-over-cable architecture is proposed to reuse cable infrastructure for femtocell deployment. It cascades cable and air channels together to implement compound MIMO processing, which requires mobile end-users to be aware of the cable related architecture. In [2], the macro network extension and densification are combined together with specific indoor small-cell solutions fronthauling through LAN cables. Our previous work [3], [4] considers a longer deploying distance—up to 300 meters from the street cabinet to the customer premises with existing telephone wires, in which case the coexistence of LTE analog fronthaul and digital subscriber line (DSL) systems is investigated.

A challenge of using the existing unshielded copper-based infrastructure is the crosstalk from the neighboring pairs due to electromagnetic coupling (as illustrated in Fig. 1). To make the infrastructure between remote radio unit (RRU) and remote radio-head (RRH) transparent to mobile end-users, crosstalk cancellation should be employed if the interference is noticeable. In the prevailing DSL systems such as VDSL2 [5], vectoring [6] is implemented to mitigate crosstalk. It applies

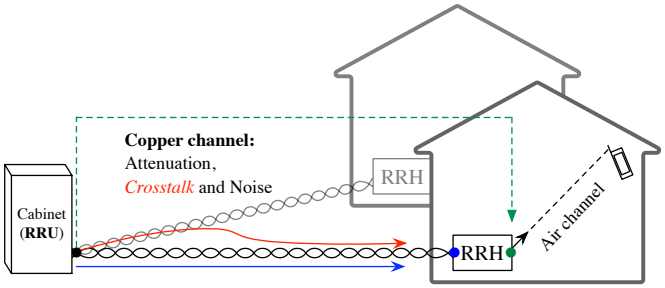

Fig. 1. Systematic sketch of LTE-over-copper in the downstream direction.

precoding in downstream and joint equalization in upstream, where the channel estimation and crosstalk cancellation techniques are typically implemented in frequency-domain.

Compared to the air channel, the copper-pair channel is more stable in time and has much higher signal-to-noise ratio (SNR). Crosstalk which was harmful to DSL signals may not be detrimental to LTE signals, as the latter are designed to cope with more severe impairments in the air channel. Depending on the cable quality, the frequency band used over copper, and the processing components inside the RRH, the need for crosstalk cancellation in LTE-over-copper (LoC) systems varies. The involved crosstalk cancellation unit should be more flexible in the sense that it can be easily turned off/on without noticeably interrupting the original LTE signal flow. Moreover, the generated LTE signal from the RRU is typically a time-domain signal, and thus implementing crosstalk cancellation also in time-domain is an appealing solution.

In [7], a time-domain precoding method is proposed for DSL systems based on fractionally-spaced filtering. It performs SNR-based coupling estimation and parameter-based multi-filter updating. Since it concerns a scenario with several digital subscriber line access multiplexers (DSLAMs), the algorithm complexity becomes unnecessarily high for our case.

In this work, we focus on far-end crosstalk (FEXT) precancellation between copper pairs sharing the same cable binder and connecting to the same RRU for LoC systems. The proposed precoding unit operates in parallel to the original LTE signal flow as interpreted in Section II. A channel impulse response (CIR) estimation method for all direct and FEXT

paths is proposed in Section III by taking advantage of LTE cell-specific reference signals (CRSs). Time-domain precoding for crosstalk cancellation and inter-symbol interference (ISI) mitigation is presented and analyzed in Section IV.

II. Precoding Architecture

At the RRU-side, signals are loaded on copper pairs with adequate transmit power for distant copper transmission. We consider a transmit power spectrum density (PSD) of $P_{\text{tx}} = -60\,\text{dBm/Hz}$ and a background noise PSD of $N_{\text{bg}} = -140\,\text{dBm/Hz}$, which result in an initial transmit $\text{SNR}_{\text{init}} = 80\,\text{dB}$. At the antenna connector of the RRH (*i.e.*, the right-hand-side of the RRH in Fig. 1), a minimum error vector magnitude (EVM) requirement for LTE signals should be achieved as discussed in [4]. Translating into SNR values, it demands around $\text{SNR}_{\text{target}} = 15.14\,\text{dB}$ for QPSK, $\text{SNR}_{\text{target}} = 18.06\,\text{dB}$ for 16-QAM, and $\text{SNR}_{\text{target}} = 21.98\,\text{dB}$ for 64-QAM. From 80 dB on one end to around 20 dB on the other end, a large SNR margin is available for the copper transmission and the implementation of the RRH.

If the SNR degradation due to FEXT over copper pairs stays within this SNR margin, we say this FEXT is tolerable and no extra effort for crosstalk cancellation is needed. Otherwise, a precoder should be involved at the RRU-side. The tolerable FEXT magnitude depends on, among other factors, the cable type, the frequency band where LTE signals are loaded, and the SNR-impacting components within the RRH. While the cable type and applied frequency determine the insertion loss of direct paths (denoted by C_{dir}), the components inside the RRH yield an overall noise figure value (denoted by NF). Consider that K RRHs share the same cable binder. To reach a certain $\text{SNR}_{\text{target}}$ for the EVM requirement, the average tolerable FEXT magnitude C_{fext} from each involved pair can be estimated as

$$C_{\text{fext}}/\text{pair} = \frac{1}{K-1}\left(\frac{C_{\text{dir}}}{\text{SNR}_{\text{target}}\cdot NF} - \frac{1}{\text{SNR}_{\text{init}}}\right), \qquad (1)$$

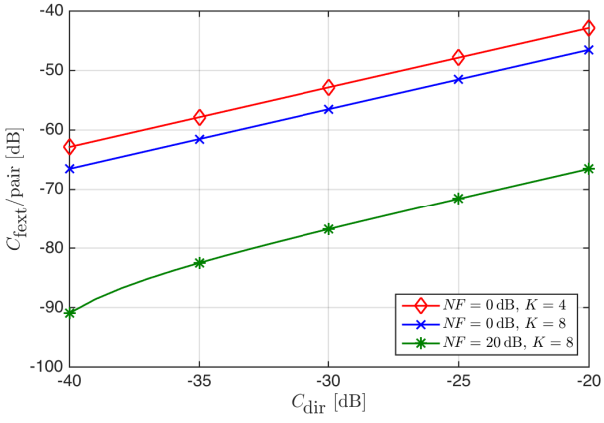

Fig. 2. Tolerable FEXT magnitude per copper pair for different system scenarios. $\text{SNR}_{\text{target}} = 18.06\,\text{dB}$ for 16-QAM is used as an example. A transmit PSD of $-60\,\text{dBm/Hz}$ and background noise PSD of $-140\,\text{dBm/Hz}$ are assumed for the copper channel.

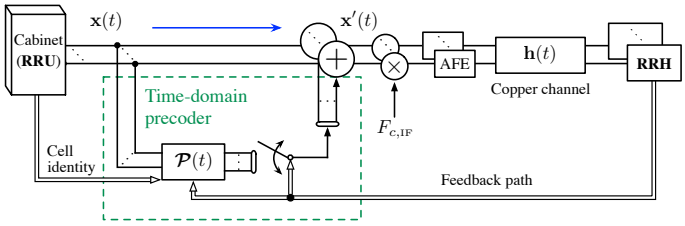

Fig. 3. Time-domain precoding architecture for LoC systems. The precoding unit can be easily turned off/on by de-/activating additive time-domain signals without any processing block located in the LTE path.

by counting every variable in linear scale. The impact of different variables in Eq. (1) on the tolerable FEXT is illustrated in Fig. 2. For example for $K = 4$, if the RRH generates $NF = 0\,\text{dB}$ and the direct channel insertion loss C_{dir} is around $-25\,\text{dB}$, no precoding is needed as long as the average FEXT from neighboring pairs is below $-50\,\text{dB}$. The tolerable value per pair reduces for a larger group size (*e.g.*, $K = 8$), which is equivalent to having more interfering sources. A noisier RRH environment with higher NF value also lowers the tolerable FEXT level as the SNR margin left for copper transmission shrinks. Thus, the need for crosstalk cancellation varies.

Since the RRU delivers LTE signals in time-domain, we propose a time-domain precoding scheme for LoC systems as illustrated in Fig. 3. Pre-compensated signals are generated by the precoder and added directly to LTE signals. Because the precoding unit is parallel to the signal path, it can be easily turned off/on based on demand without unnecessarily interrupting the original LTE signal flow.

III. Time-Domain Channel Estimation

When precoding for crosstalk cancellation is necessary, we first need to acquire prior knowledge of channel impulse responses (CIRs) for all direct and FEXT paths. In this work, we propose an error-based CIR estimation assisted by cell-specific reference signals (CRSs) [8] of the carried LTE signal.

A. LTE Cell-Specific Reference Signal (CRS) Alignment

The smallest unit of the LTE frame structure is resource element (RE). It represents one OFDM symbol in time on one sub-carrier in frequency (small squares in Fig. 4). Along the time axis, 7 OFDM symbols with normal cyclic prefix (CP) compose one slot, 2 slots compose one subframe, and 10 subframes compose one frame. A two-dimensional grid containing 1 slot in time-domain and 12 consecutive sub-carriers in frequency-domain is termed resource block (RB). A 3 MHz LTE signal, for example, has $N_{\text{rb}} = 15$ RBs corresponding to 180 sub-carriers in every slot.

In each slot there are 2 CRS-containing OFDM symbols, numbered 0 and 4 in Fig. 4(a). For symbol-0, there is one reference symbol (black square in Fig. 4) on every 6 sub-carriers. On symbol-4, the reference-symbol positions shift by 3 sub-carriers. The following slots use the same CRS mapping scheme, which forms a diamond mapping pattern to capture channel variations in frequency-domain. When applied

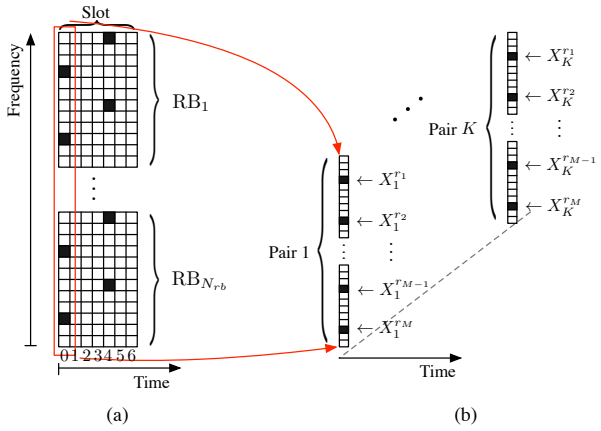

Fig. 4. Illustration of CRS-aided channel estimation. Each small square represents one RE. Each black square represents one reference symbol.

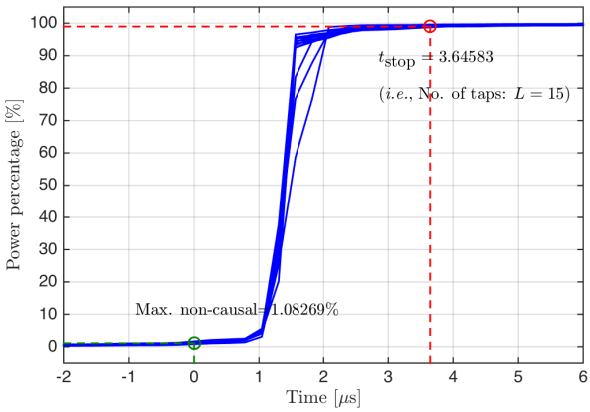

Fig. 5. Energy-based time-domain CIR truncation. For the case of $K = 4, 16$ channel paths are plotted. t_{stop} marks the time stamp for the channel spread that contains at least 99% CIR power of each path.

to estimating the copper channel which changes little in time, this kind of mapping pattern approximates to having one pilot on every 3 sub-carriers.

There are 504 different CRS sequences defined for LTE, where each sequence corresponds to one of 504 different physical-layer cell identities. Let $N_{\text{ID}}^{\text{cell}}$ denote a certain cell identity. A cell-specific frequency shift of $[N_{\text{ID}}^{\text{cell}} \mod 6]$ is applied to determine the reference-symbol positioning on the sub-carriers. Equivalently, there are only 6 possible mapping patterns that jointly cover all 504 different cell identities.

Accordingly, the baseband unit can control the CRS positioning by assigning a specific cell identity to each RRH/cell. In turn, we are essentially informed of the reference symbols and their mapping pattern contained in the coming LTE signal by knowing its cell identity. For an RRH group sharing the same cable binder, the CRS mappings can be set to be identical (as illustrated in Fig. 4(b)) by assigning their cell identities to be an integer multiple of 6 apart. For example, let cell identities be $[2, 8, 14, 26]$ for $K = 4$.

Note that small cells supported by the LoC system have low output power and are deployed in environments with high path-loss (*e.g.*, due to walls). Therefore the above reference signal alignment will not diminish pilot effectiveness due to neighboring cell interference in the air.

B. Estimation of Copper Channel Impulse Responses (CIRs)

Assume that the precoder knows the cell identities. Consider the case where LTE signals transmitted on a group of K pairs share the same CRS mapping structure. Let $\mathbf{F}_N$ denote an $N \times N$ discrete Fourier transform (DFT) matrix and $\mathbf{F}_L$ is the first L columns of $\mathbf{F}_N$, where N and L denote the DFT size and the CIR length, respectively.

The implication above that $L < N$ is generally valid in our work. To demonstrate this, we use measured frequency-domain channel data to simulate direct and FEXT couplings of a 30-pair, 300-meter, 0.5 mm cable [9] with 15 kHz sub-carrier spacing (same as LTE signals). $K = 4$ pairs are randomly picked from the same binder. The band between 21 MHz and 24 MHz (as suggested in [3]), which can fit a 3 MHz LTE signal, is studied as an example. Transforming all K^2 measured paths into time-domain with $N = 256$, Fig. 5 shows that $L = 15$ is the time-domain tap number containing at least 99% CIR power of each path. Thus, we consider a channel spread of $L = 15$ for all K^2 paths in this work.

The channel path from transmitter i to the j-th RRH can be represented by

$$\mathbf{H}_{j,i} = \mathbf{F}_L \mathbf{h}_{j,i},$$

where $\mathbf{H}_{j,i} = \left[H_{j,i}^1, \ldots, H_{j,i}^{r_1}, \ldots, H_{j,i}^{r_M}, \ldots, H_{j,i}^N\right]^T$ (including zero-padding if the number of sub-carriers is smaller than the DFT size N) denotes the frequency-domain channel representation and $\mathbf{h}_{j,i} = [h_{j,i}(0), \ldots, h_{j,i}(L-1)]^T$ denotes the time-domain CIR, respectively. Within one CRS-containing OFDM symbol as exemplified in Fig. 4, let $\mathbf{X}_i = [X_i^{r_1}, \ldots, X_i^{r_M}]^T$ denote the reference symbols sent on pair i, where M is the number of reference symbols in one OFDM symbol, and $\mathcal{R} = [r_1, \ldots, r_M]^T$ denotes the set of sub-carrier indices which are loaded with reference symbols. For a group of K RRHs/cells, transmission over copper pairs on a reference-symbol sub-carrier r_i can be modeled as

$$\begin{aligned}
\underbrace{\begin{bmatrix} Y_1^{r_i} \\ \vdots \\ Y_K^{r_i} \end{bmatrix}}_{\mathbf{Y}^{r_i}} &= \begin{bmatrix} H_{1,1}^{r_i} & \cdots & H_{1,K}^{r_i} \\ \vdots & \ddots & \vdots \\ H_{K,1}^{r_i} & \cdots & H_{K,K}^{r_i} \end{bmatrix} \begin{bmatrix} X_1^{r_i} \\ \vdots \\ X_K^{r_i} \end{bmatrix} + \mathbf{N} \\
&= \begin{bmatrix} \mathbf{F}_L^{r_i}\mathbf{h}_{1,1} & \cdots & \mathbf{F}_L^{r_i}\mathbf{h}_{1,K} \\ \vdots & \ddots & \vdots \\ \mathbf{F}_L^{r_i}\mathbf{h}_{K,1} & \cdots & \mathbf{F}_L^{r_i}\mathbf{h}_{K,K} \end{bmatrix} \begin{bmatrix} X_1^{r_i} \\ \vdots \\ X_K^{r_i} \end{bmatrix} + \mathbf{N} \\
&= \underbrace{\left[\mathbf{I}_K \otimes X_1^{r_i}\mathbf{F}_L^{r_i} \;\; \cdots \;\; \mathbf{I}_K \otimes X_K^{r_i}\mathbf{F}_L^{r_i}\right]}_{\mathbf{A}^{r_i}} \underbrace{\begin{bmatrix} \mathbf{h}_{1,1} \\ \vdots \\ \mathbf{h}_{K,1} \\ \vdots \\ \mathbf{h}_{K,K} \end{bmatrix}}_{\mathbf{h}} + \mathbf{N}, \qquad (2)
\end{aligned}$$

where $\mathbf{F}_L^{r_i}$ denotes the r_i-th row of $\mathbf{F}_L$, $\mathbf{N}$ denotes the background noise, $\mathbf{I}_K$ denotes a $K \times K$ identity matrix, $\otimes$ denotes Kronecker product, and $\mathbf{Y}^{r_i}$ denotes the receive symbols on subcarrier r_i at the RRH-side.

Observe in Eq. (2) that the unknown vector $\mathbf{h}$ is frequency independent, which connects the reference-symbol-containing matrix $\mathbf{A}^{r_i}$ to the receive signal $\mathbf{Y}^{r_i}$ on each reference-symbol sub-carrier r_i. Stacking and interleaving all the information collected from the M reference-symbol sub-carriers yield

$$\underbrace{\begin{bmatrix}\mathbf{Y}_1^T & \cdots & \mathbf{Y}_K^T\end{bmatrix}^T}_{\mathbf{y}} = \underbrace{\begin{bmatrix}\mathbf{A}_1 & \cdots & \mathbf{A}_K\end{bmatrix}}_{\mathbf{A}}\mathbf{h} + \mathbf{N}, \tag{3}$$

where $\mathbf{Y}_i = [Y_i^{r_1}, \ldots, Y_i^{r_M}]^T$ and

$$\mathbf{A}_i = \mathbf{I}_K \otimes \begin{bmatrix} X_i^{r_1}\mathbf{F}_L^{r_1} \\ \vdots \\ X_i^{r_M}\mathbf{F}_L^{r_M} \end{bmatrix}.$$

To make the rank of $\mathbf{A}$ in Eq. (3) equal the dimension of its column space and also to average out the noise influence, we extend $\mathbf{y}$ and $\mathbf{A}$ in Eq. (3) vertically by stacking more $\mathbf{Y}_i$ and $\mathbf{A}_i$ from the following CRS-containing OFDM symbols yielding $\bar{\mathbf{y}}$ and $\bar{\mathbf{A}}$. The K^2 CIRs, which are vertically stacked in one column vector $\mathbf{h}$ can be estimated by

$$\widehat{\mathbf{h}} = \left(\bar{\mathbf{A}}^{\mathrm{H}}\bar{\mathbf{A}}\right)^{-1}\bar{\mathbf{A}}^{\mathrm{H}}\bar{\mathbf{y}}. \tag{4}$$

Since the CRS related matrix $\bar{\mathbf{A}}$ in Eq. (4) can be directly generated from the corresponding cell identities and $\bar{\mathbf{y}}$ is fed back from RRHs, the whole estimation process can be accomplished without interrupting the LTE signal flow.

IV. Time-Domain Precoding

The proposed time-domain precoder includes two functional parts: crosstalk cancellation and ISI mitigation.

A. Crosstalk Cancellation

With the estimated $\widehat{\mathbf{h}}$ in Eq. (4), we can reconstruct it into the direct-and-FEXT-path format as

$$\boldsymbol{\mathcal{H}} = \begin{bmatrix} \widehat{\mathbf{h}}_{1,1} & \cdots & \widehat{\mathbf{h}}_{1,K} \\ \vdots & \ddots & \vdots \\ \widehat{\mathbf{h}}_{K,1} & \cdots & \widehat{\mathbf{h}}_{K,K} \end{bmatrix},$$

where each entry $\widehat{\mathbf{h}}_{j,i}$ denotes a length-L time-domain impulse response from the i-th transmitter to the j-th RRH. In this case, $\boldsymbol{\mathcal{H}}$ is essentially a three-dimensional matrix.

Similar to the normal two-dimensional matrix case, it is shown in [10] that the following relation exists for $\boldsymbol{\mathcal{H}}$:

$$\boldsymbol{\mathcal{H}} * \mathrm{adj}(\boldsymbol{\mathcal{H}}) = \det(\boldsymbol{\mathcal{H}}) * \boldsymbol{\mathcal{I}}, \tag{5}$$

where $*$ denotes the convolutional operator and $\boldsymbol{\mathcal{I}}$ is a diagonal matrix with each diagonal entry being a Dirac delta function $\boldsymbol{\delta}$. Similar to the Leibniz formula for the determinant of a two-dimensional matrix, $\det(\boldsymbol{\mathcal{H}})$ in Eq. (5) is defined by

$$\det(\boldsymbol{\mathcal{H}}) = \sum_{\sigma \in S_K} \mathrm{sgn}(\sigma) \overset{K}{\underset{i=1}{*\prod}} \mathbf{h}_{i,\sigma_i},$$

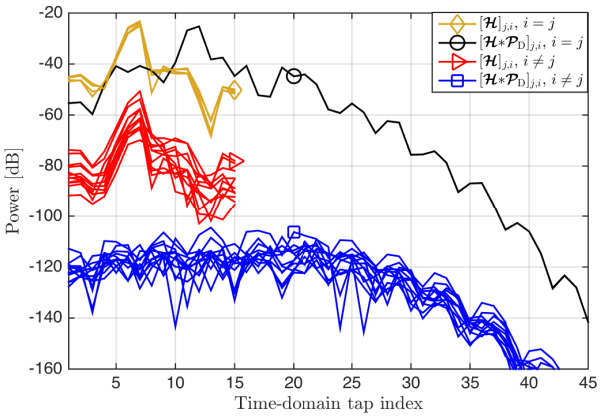

Fig. 6. Equivalent CIRs before and after performing the time-domain diagonalizing precoding. A delay of $\Delta = 13$ taps is considered after precoding. Matrix entries with $i = j$ indicate direct paths, while entries with $i \neq j$ indicate FEXT paths.

where $\overset{*}{\prod}$ denotes a series of convolution instead of multiplication, σ is one permutation vector out of the permutation group S_K, and $\mathrm{sgn}(\sigma)$ is the signature of σ that calculates the determinant of corresponding permutation matrix. The permutation group S_K contains all possible permutations of $[1, \ldots, K]$. Each entry of the adjoint matrix is defined accordingly as

$$[\mathrm{adj}(\boldsymbol{\mathcal{H}})]_{i,j} = (-1)^{i+j}\det\left(\boldsymbol{\mathcal{H}}_{(j,i)}\right), \tag{6}$$

where $\boldsymbol{\mathcal{H}}_{(j,i)}$ denotes the (j,i) minor of $\boldsymbol{\mathcal{H}}$ that deletes j-th row and i-th column from $\boldsymbol{\mathcal{H}}$.

Assign the time-domain diagonalizing precoder to be $\boldsymbol{\mathcal{P}}_{\mathrm{D}} = \mathrm{adj}(\boldsymbol{\mathcal{H}})$. Disregarding the transmit power limitation for now, the receive signal in time-domain becomes

$$\begin{aligned}\boldsymbol{\mathcal{Y}} &= \boldsymbol{\mathcal{H}} * \boldsymbol{\mathcal{P}}_{\mathrm{D}} * \boldsymbol{\mathcal{X}} + \boldsymbol{\mathcal{N}} \\ &= \det(\boldsymbol{\mathcal{H}}) * \boldsymbol{\mathcal{I}} * \boldsymbol{\mathcal{X}} + \boldsymbol{\mathcal{N}},\end{aligned} \tag{7}$$

where $\boldsymbol{\mathcal{X}} = [\mathbf{x}_1, \ldots, \mathbf{x}_K]^{\mathrm{T}}$, and $\mathbf{x}_i$ denotes the time-domain LTE signal transmitted on pair i. The receive signal $\boldsymbol{\mathcal{Y}} = [\mathbf{y}_1, \ldots, \mathbf{y}_K]^{\mathrm{T}}$ and background noise $\boldsymbol{\mathcal{N}}$ are defined similarly.

Note that $\det(\boldsymbol{\mathcal{H}})$ in Eq. (7) is *one* CIR with length $KL - (K-1)$. The term $\det(\boldsymbol{\mathcal{H}}) * \boldsymbol{\mathcal{I}}$ implies that the effective channel after precoding has *identical* CIR on every direct path, while FEXT is zeroed out. The $\boldsymbol{\mathcal{P}}_{\mathrm{D}}$ implemented to generate results in Fig. 6 is constructed based on the estimated CIRs using Eq. (4) with 10 slots of CRS. It is observed that the effective direct CIRs (see black circle-marked lines in Fig. 6) are identical and the FEXT paths (blue square-marked lines) are effectively suppressed to much lower power levels compared to the original FEXT paths (red triangle-marked lines).

B. Inter-Symbol Interference (ISI) Mitigation

One outcome of the precoding scheme in Section IV-A is that the direct channel spread is extended from L to $KL - (K-1)$ (also shown in Fig. 6 when comparing the yellow diamond-marked lines to the black circle-marked lines).

The short version of LTE CP duration is $4.6875\,\mu$s, whereas 90% of indoor delay spread is below 500 ns (see Table 5 in [11]). It implies that at least 85% of the LTE CP length can be consumed by the transmission over copper pairs. If the effective copper channel spread after applying $\mathcal{P}_{\text{D}}$ is longer than this CP portion, it is worthwhile introducing further spread-confining filters in the precoder to mitigate ISI.

As the time-domain channel representation is a finite impulse response (FIR), full equalization aiming for a Dirac delta function will require an infinite impulse response (IIR) filter. In practice, we compromise by only confining the direct channel spread to be shorter than the reserved CP length for copper transmission. In [12], an optimal shortening filter is proposed which maximizes the shortening SNR (SSNR). Since all K direct paths are the same after applying $\mathcal{P}_{\text{D}}$, it is sufficient to design a single shortening filter.

Let $\mathbf{w}$ denote the impulse response shortening (IRS) filter with length L_{IRSF}. Let $\mathbf{H}_{\text{conv}}$ denote the convolutional matrix of $\det(\boldsymbol{\mathcal{H}})$ and let $\mathbf{h}_{\text{prec}}$ denote the effective direct CIR after implementing the complete time-domain precoding, *i.e.*,

$$\mathbf{h}_{\text{prec}} = \det(\boldsymbol{\mathcal{H}}) * \mathbf{w} = \mathbf{H}_{\text{conv}}\mathbf{w}.$$

With a certain amount of delay Δ considered and a shortened CIR length of L_{target} targeted, the objective part of $\mathbf{h}_{\text{prec}}$ that has effective CIR values is given by

$$\mathbf{h}_{\text{eff}} = \mathbf{Z}_{\text{eff}}\mathbf{h}_{\text{prec}} = \mathbf{H}_{\text{eff}}\mathbf{w},$$

where $\mathbf{H}_{\text{eff}} = \mathbf{Z}_{\text{eff}}\mathbf{H}_{\text{conv}}$ and

$$\mathbf{Z}_{\text{eff}} = \begin{bmatrix}\mathbf{0}_{L_{\text{target}}\times(\Delta-1)} & \mathbf{I}_{L_{\text{target}}} & \mathbf{0}_{L_{\text{target}}\times(KL-K+L_{\text{IRSF}}-L_{\text{target}}-\Delta+1)}\end{bmatrix}$$

is a matrix that picks the rows $\mathcal{T} = [\Delta, \ldots, \Delta + L_{\text{target}} - 1]$ from a matrix/vector. Similarly, the rest of $\mathbf{h}_{\text{prec}}$ is denoted by

$$\mathbf{h}_{\text{rest}} = \mathbf{Z}_{\text{rest}}\mathbf{h}_{\text{prec}} = \mathbf{H}_{\text{rest}}\mathbf{w},$$

where $\mathbf{H}_{\text{rest}} = \mathbf{Z}_{\text{rest}}\mathbf{H}_{\text{conv}}$ and $\mathbf{Z}_{\text{rest}}$ picks the rows $[1, \ldots, KL-K+L_{\text{IRSF}}]\backslash\mathcal{T}$ from a matrix/vector. Accordingly, the energy inside and outside the chunk of interest is formulated respectively as

$$\mathbf{h}_{\text{eff}}^{\text{H}}\mathbf{h}_{\text{eff}} = \mathbf{w}^{\text{H}}\mathbf{H}_{\text{eff}}^{\text{H}}\mathbf{H}_{\text{eff}}\mathbf{w} = \mathbf{w}^{\text{H}}\mathbf{B}\mathbf{w},$$
$$\mathbf{h}_{\text{rest}}^{\text{H}}\mathbf{h}_{\text{rest}} = \mathbf{w}^{\text{H}}\mathbf{H}_{\text{rest}}^{\text{H}}\mathbf{H}_{\text{rest}}\mathbf{w} = \mathbf{w}^{\text{H}}\mathbf{C}\mathbf{w},$$

TABLE I
MAXIMUM SSNR SHORTENING IMPULSE RESPONSE FILTER

	$L_{\text{target}} >= L_{\text{IRSF}}$	$L_{\text{target}} < L_{\text{IRSF}}$
Eigen-decomp.	$\mathbf{B} = \mathbf{Q}\boldsymbol{\Sigma}\mathbf{Q}^{\text{H}}$	$\mathbf{B} = \begin{bmatrix}\mathbf{U} & \mathbf{V}\end{bmatrix}\begin{bmatrix}\boldsymbol{\Sigma} & \mathbf{0}\\ \mathbf{0} & \mathbf{0}\end{bmatrix}\begin{bmatrix}\mathbf{U}^{\text{H}}\\ \mathbf{V}^{\text{H}}\end{bmatrix}$
$\mathbf{D}$	$(\sqrt{\mathbf{B}})^{-1}\mathbf{C}(\sqrt{\mathbf{B}}^{\text{H}})^{-1}$	$(\boldsymbol{\Lambda}^{\text{H}} - \boldsymbol{\Lambda}^{\text{H}}\mathbf{O}^{\text{H}})\mathbf{C}(\boldsymbol{\Lambda} - \mathbf{O}\boldsymbol{\Lambda})$ for $\mathbf{O} = \mathbf{V}(\mathbf{V}^{\text{H}}\mathbf{C}\mathbf{V})^{-1}\mathbf{V}^{\text{H}}\mathbf{C}$, and $\boldsymbol{\Lambda} = \mathbf{U}(\sqrt{\boldsymbol{\Sigma}})^{-1}$.
$\mathbf{q}_{\min}$	Eigenvector of the minimum eigenvalue $\lambda_{\min}$ of $\mathbf{D}$.	
$\mathbf{w}_{\text{opt}}$	$(\sqrt{\mathbf{B}})^{-1}\mathbf{q}_{\min}$	$(\mathbf{I} - \mathbf{O})\boldsymbol{\Lambda}\mathbf{q}_{\min}$

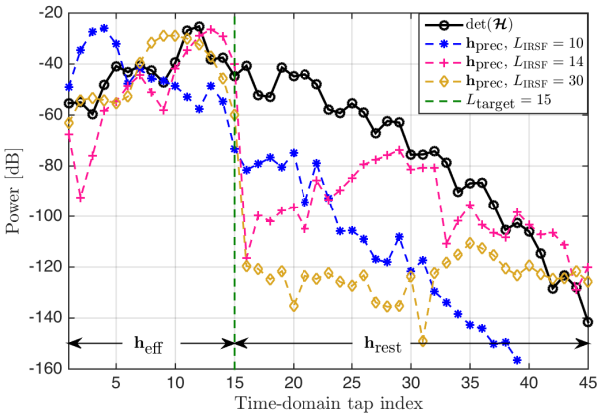

(a) Time-domain channel representation.

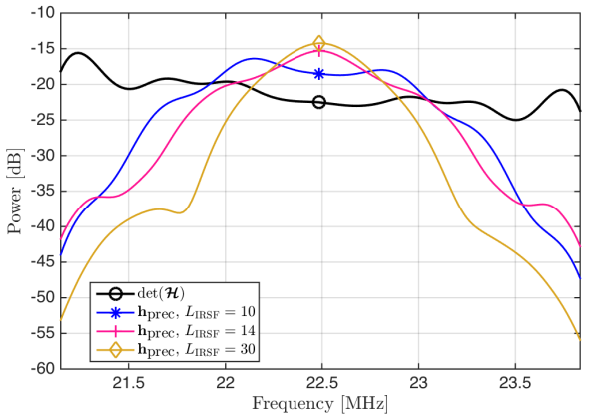

(b) Frequency-domain channel representation.

Fig. 7. Direct channel IRS for $L_{\text{target}} = 15$, considering channel measurements between 21 MHz and 24 MHz. A delay of $\Delta = 13$ taps is considered after precoding.

where $\mathbf{B} = \mathbf{H}_{\text{eff}}^{\text{H}}\mathbf{H}_{\text{eff}}$ and $\mathbf{C} = \mathbf{H}_{\text{rest}}^{\text{H}}\mathbf{H}_{\text{rest}}$. Implementing eigen-decomposition as in [12] and summarized in Table I, the optimal IRS filter $\mathbf{w}_{\text{opt}}$ can be obtained in the sense of maximizing the SSNR $= \frac{\mathbf{w}^{\text{H}}\mathbf{B}\mathbf{w}}{\mathbf{w}^{\text{H}}\mathbf{C}\mathbf{w}}$ as

$$\mathbf{w}_{\text{opt}} = \arg\max_{\mathbf{w}} \left[\frac{\mathbf{w}^{\text{H}}\mathbf{B}\mathbf{w}}{\mathbf{w}^{\text{H}}\mathbf{C}\mathbf{w}}\right].$$

The length relation between L_{target} and L_{IRSF} differentiated in Table I determines the singularity of matrix $\mathbf{B}$.

Fig. 7 reveals that there is a trade-off between the time-domain shortening effectiveness and the frequency-domain effective channel gain. A longer shortening filter (*e.g.*, $L_{\text{IRSF}} = 30$, yellow diamond-marked line in Fig. 7a) suppresses the channel spread outside L_{target} to a much lower level compared to a shorter filter (*e.g.*, $L_{\text{IRSF}} = 10$, blue star-marked line). The counterparts in frequency-domain in Fig. 7b show that the effective channel using a shorter filter (*e.g.*, $L_{\text{IRSF}} = 10$) has a higher channel gain over the 3 MHz bandwidth compared to that of a longer filter (*e.g.*, $L_{\text{IRSF}} = 30$). Since the time-domain spread affects the ISI and the frequency-domain effective channel gain affects the receive signal power, using a longer L_{IRSF} does not necessarily result in a higher receive SNR. The

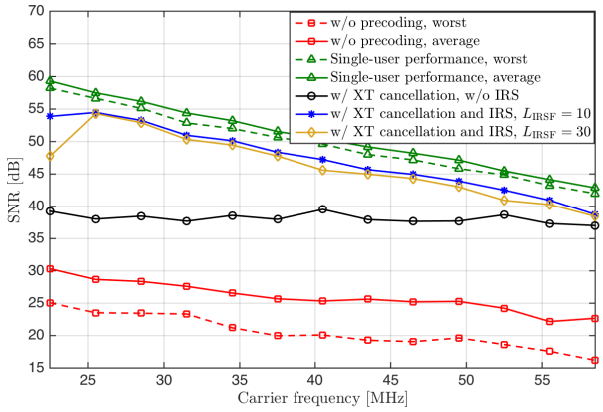

Fig. 8. Receive SNR comparison at the copper and RRH connecting point.

effect of this trade-off is illustrated in terms of SNR in the next subsection.

In summary, the time-domain precoder is formulated as

$$\boldsymbol{\mathcal{P}} = \mu \cdot \mathrm{adj}(\boldsymbol{\mathcal{H}}) * \mathbf{w}', \tag{8}$$

where $\mathrm{adj}(\boldsymbol{\mathcal{H}})$ diagonalizes the interference channel as defined in Eq. (6). $\mathbf{w}' = \mathbf{w}_{\mathrm{opt}}$ is the filter given by Table I if the direct CIR shortening is needed; otherwise $\mathbf{w}' = \boldsymbol{\delta}$. The power normalization factor μ that constrains the transmit power is defined as

$$\mu = \frac{1}{\max\limits_{i\in[1,\ldots,K]} \sum_{j=1}^{K} \left\| [\mathrm{adj}(\boldsymbol{\mathcal{H}}) * \mathbf{w}']_{i,j} \right\|_2}.$$

C. Precoding Simulation Results

In Fig. 8, the average receive SNR is calculated over a 3 MHz band. The carrier frequency of each band is shifted from 22.5 MHz (referring to a band 21 MHz–24 MHz) to 58.5 MHz (referring to a band 57 MHz–60 MHz) to study the impact of different channel characteristics. A flat transmit PSD of -60 dBm/Hz is applied and a copper channel background noise PSD of -140 dBm/Hz is assumed. The data symbols are 16-QAM modulated as an example.

The single-user performance is calculated as a reference using only the direct-path measurements. No crosstalk and transmit power constraint is considered. It can be viewed as an ideal situation after precoding. For the single-user and the crosstalk-corrupted performances in Fig. 8, average and worst situations are presented, respectively. For the other lines that have the time-domain crosstalk cancellation (as in Section IV-A) implemented, the receive SNR for one RRH is presented since we show in Fig. 6 that the crosstalk is effectively suppressed and the direct paths are identical.

Whether or not the IRS filter should be added is also implementation dependent. If the SNR result without IRS (*e.g.*, the black circle-marked line in Fig. 8) is already acceptable, there is no need to add the IRS filter which changes the shape of the frequency-domain equivalent channel as shown in Fig. 7b and may increase the complexity of the frequency-domain equalizer. Especially when considering a higher frequency range where the direct coupling magnitude decreases, the SNR difference among the single-user performance, the precoded performances with and without IRS becomes much smaller.

V. Conclusion

Time-domain crosstalk cancellation provides more flexibility and is less intrusive than traditional vectoring for LTE-over-copper (LoC) systems. The proposed approach exploits LTE reference signals to estimate the copper channel, cancels crosstalk, and yields effective direct paths that are identical for all pairs. The latter enables low-complexity channel shortening in case the desired receive SNR at the RRH-side is not achieved because of the direct channel spread. Simulation results with measured copper channel data confirm that the precoder performance is close to the single-user bound.

Acknowledgement

This work was partly supported by the Celtic-Plus project GOLD, the EU H2020 5G-Crosshaul project (grant no. 671598) and the EXAM project of EIT Digital.

References

[1] J. Gambini and U. Spagnolini, "Wireless Over Cable for Femtocell Systems," *IEEE Communications Magazine*, vol. 51, no. 5, pp. 178–185, May 2013.

[2] C. Lu, M. Berg, E. Trojer, P.-E. Eriksson, K. Laraqui, O. V. Tidblad, and H. Almeida, "Connecting the dots: small cells shape up for high-performance indoor radio," *Ericsson Review*, vol. 91, December 2014. [Online]. Available: http://goo.gl/YvdY5N

[3] Y. Huang, E. Medeiros, S. Höst, T. Magesacher, P.-E. Eriksson, C. Lu, P. Ödling, and P. O. Börjesson, "Enabling DSL and Radio on the Same Copper Pair," in *Proc. 2015 IEEE International Conference on Communications (ICC)*, June 2015, pp. 1031–1035.

[4] Y. Huang, E. Medeiros, N. Fonseca, S. Höst, T. Magesacher, P.-E. Eriksson, C. Lu, P. Ödling, and P. Börjesson, "LTE over Copper – Potential and Limitations," in *Proc. 2015 IEEE 26th Annual International Symposium on Personal, Indoor, and Mobile Radio Communications (PIMRC)*, August 2015, pp. 1339–1343.

[5] ITU, "Very High Speed Digital Subscriber Line Transceivers 2 (VDSL2)," Recommendation ITU-T G.993.2, December 2011. [Online]. Available: https://www.itu.int/rec/T-REC-G.993.2-201112-I/en

[6] G. Ginis and J. Cioffi, "Vectored Transmission for Digital Subscriber Line Systems," *IEEE Journal on Selected Areas in Communications*, vol. 20, no. 5, pp. 1085–1104, 2002.

[7] F. A. Mruck, C. Stierstorfer, J. B. Huber, and R. Tzschoppe, "Time-Domain MIMO Precoding for FEXT Cancellation in DSL Systems," in *Proc. 2013 17th International ITG Workshop on Smart Antennas (WSA)*, March 2013, pp. 1–7.

[8] 3GPP, "LTE; Evolved Universal Terrestrial Radio Access (E-UTRA); Physical channels and modulation," 3rd Generation Partnership Project (3GPP), TS 36.211 V12.6.0, July 2015. [Online]. Available: http://goo.gl/jepG09

[9] Ericsson AB, *Access Network Pair cable, TEL 312*, 2010. [Online]. Available: http://goo.gl/4RdCXc

[10] E. Auger, B. Rankov, M. Kuhn, and A. Wittneben, "Time Domain Precoding for MIMO-OFDM Systems," in *Proc. 10th International OFDM-Workshop*, August 2005.

[11] ITU-R, "Propagation data and prediction methods for the planning of indoor radiocommunication systems and radio local area networks in the frequency range 300 MHz to 100 GHz," International Telecommunication Union (ITU), Recommendation P.1238-8, July 2015. [Online]. Available: https://goo.gl/UG1HmB

[12] P. Melsa, R. Younce, and C. Rohrs, "Impulse Response Shortening for Discrete Multitone Transceivers," *IEEE Transactions on Communications*, vol. 44, no. 12, pp. 1662–1672, December 1996.